Comprehensive Genetic Analysis Unraveled the Missing Heritability and a Founder Variant of *BEST1* in a Chinese Cohort With Autosomal Recessive Bestrophinopathy

Jie Shi, Lu Tian, Tengyang Sun, Xiao Zhang, Ke Xu, Yue Xie, Xiaoyan Peng, Xin Tang, Zi-Bing Jin, and Yang Li

Beijing Institute of Ophthalmology, Beijing Tongren Eye Center, Beijing Tongren Hospital, Capital Medical University, Beijing Ophthalmology & Visual Sciences Key Lab, Beijing, China

Correspondence: Yang Li, Beijing Institute of Ophthalmology, Beijing Tongren Eye Center, Beijing Tongren Hospital, Hougou Lane 17, Chong Nei Street, Beijing 100730, China; yilbio@163.com.

Received: April 18, 2023
Accepted: September 2, 2023
Published: September 25, 2023

Citation: Shi J, Tian L, Sun T, et al. Comprehensive genetic analysis unraveled the missing heritability and a founder variant of *BEST1* in a Chinese cohort with autosomal recessive bestrophinopathy. *Invest Ophthalmol Vis Sci.* 2023;64(12):37. https://doi.org/10.1167/iovs.64.12.37

Purpose. To describe the genetic landscape of *BEST1* for a large Chinese cohort with autosomal recessive bestrophinopathy (ARB), identify the missing heritability, and report a common Chinese founder variant.

Methods. We recruited 65 patients from 63 families with a clinical diagnosis of ARB. All patients underwent ophthalmic examinations and comprehensive genetic analyses, including Sanger DNA sequencing of *BEST1* and whole genome sequencing (WGS). The effects of deep intronic variants (DIVs) on splicing were assessed using in vitro splicing assays in HEK293T cells and patient-derived peripheral blood mononuclear cells. Haplotype mapping was performed for 17 unrelated patients harboring variant c.867+97G>A.

Results. We identified 54 distinct disease-causing variants of *BEST1* in 63 pedigrees, 62 probands with biallelic variants, and one family with monoallelic variants. Sanger DNA sequencing of *BEST1* initially detected 51 variants in 61 pedigrees, including 19 probands with one heterozygous variant. Subsequent WGS, combined with supplementary Sanger sequencing, revealed three missing DIVs (c.1101-491A>G, c.867+97G>A, and c.867+97G>T) in 20 families. The novel DIV c.1101-491A>G caused an abnormal splicing resulting in a 204-nt pseudoexon (PE) insertion, whereas c.867+97G>A/T relatively strengthened an alternative donor site, resulting in a 203-nt intron retention (IR). The PE and IR generated a premature termination codon downstream. Haplotype analysis identified c.867+97G>A as a common founder variant with an allele frequency of 16%.

Conclusions. Our results expand the pathogenic variant spectrum of *BEST1*, and DIVs can explain almost all of the missing heritability. The c.867+97G>A DIV is a common founder variant for Chinese patients with ARB.

Keywords: *BEST1*, deep intronic variant, founder variant

Autosomal recessive bestrophinopathy (ARB, MIM 611809), first described by Burgess et al.[1] in 2008, is caused by biallelic *BEST1* pathogenic variants. ARB is characterized by subretinal yellowish fleck deposits scattered around the vascular arcades and extending to the mid-peripheral retina. These deposits correspond to hyperautofluorescence on fundus autofluorescence (FAF) images and are accompanied by retinoschisis or subretinal fluid (SRF). Patients with ARB usually have short axial length, hyperopia, and a shallow anterior chamber.[2] Electrooculography (EOG) is critical for the clinical diagnosis of ARB and is characterized by a decreased Arden ratio (light peak/dark trough) of less than 1.5 due to severe generalized retinal pigment epithelium (RPE) dysfunction.[1,2]

The *BEST1* gene is located on chromosome 11q13 and encodes a 585-amino-acid (aa) transmembrane protein referred to as bestrophin 1.[1] Bestrophin 1 is a pentameric calcium-activated chloride channel predominantly expressed in the basolateral plasma membrane of the RPE, where it plays a vital role in RPE physiological function. Bestrophin 1 regulates the flow of chloride and other anions according to intracellular calcium concentrations, although the exact mechanism remains unclear.[3–5] To date, 416 *BEST1* variants have been recorded in the Human Gene Mutation Database (Professional 2023.1), and patients with these variants present four retinal degeneration phenotypes, collectively referred to as "bestrophinopathies." In addition to ARB, the other bestrophinopathies are Best vitelliform macular dystrophy (BVMD),[6] adult-onset vitelliform macular dystrophy,[7] and autosomal dominant vitreoretinochoroidopathy,[8] all of which are inherited as autosomal dominant (AD) traits. Over 80% (334/416) of the variants in *BEST1* are missense, and 70.3% of the missense variants have been detected in patients with dominant bestrophinopathies. By contrast, 98.4% of the truncated variants have been identified in patients with ARB.[9]

Several previous studies, including one of our own, reported that 14% to 59% of patients clinically diagnosed with ARB have only one or even no identified *BEST1* variant.[10–12] Xuan et al.[11] even proposed that ARB might be

a clinical phenotype with a different inheritance model, rather than an autosomal recessive pattern. The disclosure of increasingly more missing heritability in noncoding regions or by structural variations in other inherited retinal dystrophy genes, such as *USH2A* or *ABCA4*,[13,14] has emphasized the necessity of comprehensive genetic analysis to reveal the missing variants of *BEST1* for patients with ARB who carry only monoallelic variants or have no variant detected.

In the current study, we conducted a comprehensive molecular analysis of 65 patients from 63 unrelated families with suspected ARB. Whole genome sequencing (WGS) revealed three missing alleles. Minigene analysis confirmed one novel deep intronic variant (DIV), resulting in the insertion of a pseudoexon (PE) and another two DIVs causing intron retentions (IRs). We also identified a founder variant c.867+97G>A that accounted for approximately 16% of the heritability in Chinese patients with ARB.

Methods

Participants

A total of 65 patients from 63 pedigrees were recruited from the Genetics Laboratory of the Beijing Institute of Ophthalmology, Beijing Tongren Ophthalmic Center, from 2011 to 2022. All enrolled patients were clinically diagnosed with ARB, and 21 were described in our previous study.[10] The enrolled patients met the following two criteria: (1) hyperautofluorescence in FAF corresponding to multifocal subretinal vitelliform deposits and subretinal and intraretinal fluid, and (2) carrying at least one causative *BEST1* variant. Of the 65 enrolled patients, 61 were of Chinese Han ethnicity, three from one pedigree were of Mongolian ethnicity, and one was Tibetan. Of the 63 probands, four were from consanguineous marriages and 52 were sporadic patients.

All patients underwent comprehensive ophthalmic examinations, including best-corrected visual acuity, slit-lamp biomicroscopy, color fundus photography, and optical coherence tomography (OCT); most of them also underwent fundus FAF and EOG. The study adhered to the tenets of the Declaration of Helsinki and received ethical approval from the Beijing Tongren Hospital Joint Committee on Clinical Investigation (Beijing, China). All participants or their guardians provided written informed consent.

PCR-Based Sequencing of the *BEST1* Gene

We collected peripheral blood samples from all patients and their available relatives and then extracted genomic DNA using genomic DNA extraction and purification kits (Cwbio, Beijing, China) following the manufacturer's protocol. All 11 exons and the flanking splice site of the *BEST1* gene were amplified by polymerase chain reaction (PCR) using the primers listed in Supplementary Table S1. The purified PCR amplicons were directly sequenced on an ABI Prism 373A DNA sequencer (Applied Biosystems, Foster City, CA, USA). The results were compared to the *BEST1* transcript NM_004183.4. Co-segregation analysis was performed whenever possible.

WGS, Supplementary PCR-Based Sequencing, and Bioinformatics Analysis

Twenty-three patients (21 families) had only one variant or no variant identified after Sanger sequencing. We performed

Table 1. Splice Prediction Analysis of Three Deep Intronic Variants (DIVs) Identified in This Study

Nucleotide Change	Human Splicing Finder (0–100)				MaxEntScan (0–12)				NetGene2 (0-1)				NNSplice (0-1)				Alternative Splice Site Predictor (0–12)			
	WT	MT	MT_S	DV%	WT	MT	MT_S	DV%	WT	MUT	MT_S	DV%	WT	MT	MT_S	DV%	WT	MT	MT_S	DV%
c.1101-491A>G	68.43	95.57	95.6%*	27.1	0.71	8.89	74.1%*	68.2*	ND	0.81	81.0%*	—	ND	0.93	93.0%*	—	4.293	10.456	87.1%*	51.4*
c.867+97G>A	ND	ND	—	—	ND	ND	—	—	ND	ND	—	—	ND	ND	—	—	ND	ND	—	—
c.867+97G>T	ND	ND	—	—	ND	ND	—	—	ND	ND	—	—	ND	ND	—	—	ND	ND	—	—

WT, wild type; MT, mutant type; MT_S, MT strength compared to the maximal score; DV, difference value, the increased splice prediction scores of the MT compared to the WT; ND, not detected.

*The scores met the splicing site screening criteria.

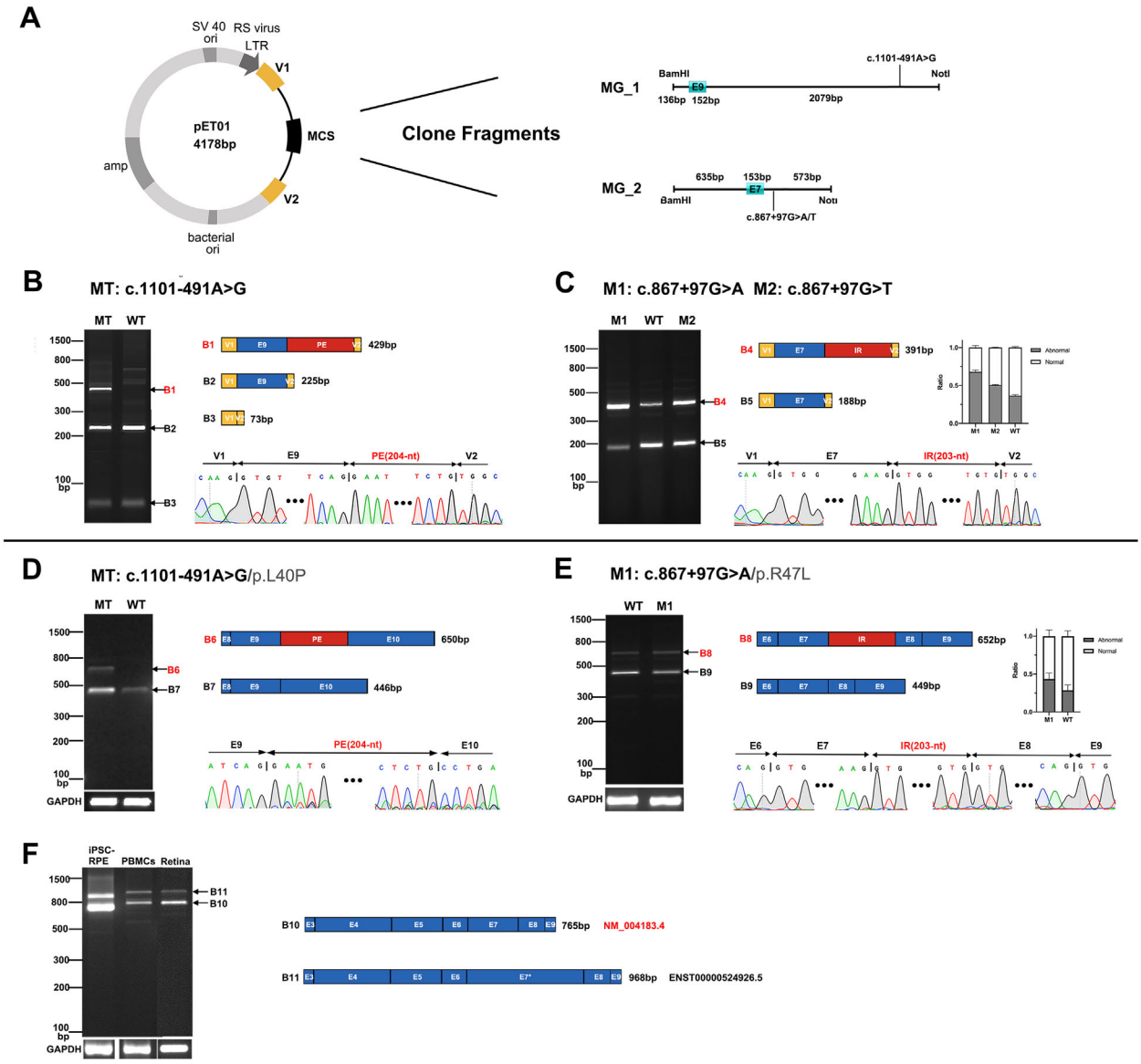

Figure 1. Outline of splice defects due to three DIVs in *BEST1*. Reverse transcription–polymerase chain reaction (RT-PCR) analysis from minigene assay transfected into HEK-293T cells (**A**–**C**) and patient-derived peripheral blood mononuclear cells (PBMCs), human retina, and induced pluripotent stem cell-derived (iPSC)-retinal pigment epithelium (RPE) cells (**D**–**F**). (**A**) Schematic representation of the two groups of minigenes that were cloned between exons V1 and V2 in pET01. The positions of the variants present in the two minigenes are indicated. (**B**) RT-PCR products of MG_1 containing c.1101-491A>G variant. One defect (fragment B1) was observed next to the WT fragment (B2). A 204-nt pseudoexon (PE) inclusion was detected in the mutant type (MT) constructs when compared with the WT. (**C**) RT-PCR products of MG_2 containing c.867+97G>A and c.867+97G>T variants. Two fragments appear in all three lanes (B4 and B5). A 203-nt intron retention (IR) was detected in abnormal product B4. Proportions of the abnormal transcript (B4) were 67.7%, 50.0%, and 37.5% in total transcripts for DIV c.867+97G>A, c.867+97G>T, and WT constructs, respectively. (**D**) RT-PCR products of PBMCs from the patient carrying c.1101-491A>G/p.L40P and a normal control. One defect (fragment B6) containing a 204-nt PE was observed. (**E**) RT-PCR products of PBMCs derived from a patient carrying c.867+97G>A/p.R47L and a normal control. Two fragments appeared in both lanes (B8 and B9), with a 203-nt IR detected in the abnormal product B8. Proportions of abnormal transcript (B8) were 44.4% and 28.6%, respectively, for PBMCs from the patient harboring c.867+97G>A/p.R47L and normal control. (**F**) RT-PCR results from human retina, iPSC-RPE, and PBMCs all displayed two transcript products (B10 and B11), of which B10 (765bp) corresponded to the transcript NM_004183.4 and B11 (968bp) corresponded to ENST00000524926.5. E7* indicates the longer exon7 in ENST00000524926.5.

WGS for seven patients (010229, 010387, 010408, 010345, 010740, 113910, and 113912) using MGI to detect the missing variants. The WGS libraries were sequenced on the DNBSEQ-T7 platform using a 100-bp paired-end mode with 30-fold minimal median coverage per genome. The sequencing data were analyzed as described previously.[15] Variant c.867+97G>A was detected in four of the seven patients in WGS; therefore, we performed supplementary Sanger sequencing to screen this variant in the remaining 16 patients.

Five algorithms, namely Human Splicing Finder (v2.4.1), NetGene2 (v2.42), MaxEntScan (v2003-7-22), Alternative Splice Site Predictor (v3.1), and NNSplice (v0.9), were applied to evaluate the probability that DIVs would cause

aberrant splicing effects. Variants were chosen for further minigene assays when they were located at putative splice sites with a relative strength of at least 60% of the maximal score in at least two of five splice prediction programs or when they led to an increased splice prediction score of at least 30% compared to the wild type (WT).

Minigene Assay and Reverse Transcription PCR Analysis

Three DIVs (c.1101-491A>G, c.867+97G>A, and c.867+97G>T) were evaluated with the pET01-based exon trapping system (Exontrap; MoBiTec GmbH, Goettingen, Germany) for possible influences on splicing. The novel DIV c.1101-491A>G was highly implicated in splicing abnormality by all five algorithms (Table 1). The DIVs c.867+97G>A/T detected in 19 patients co-segregated with their phenotype and presented in very low frequencies in the public databases; therefore, we conducted minigene analysis even though no splicing abnormality was predicted for them by any of the five algorithms (Table 1, Supplementary Fig. S1). The cloned sequences, including each DIV, as well as the upstream exon and downstream intron, were cloned into the pET01 vector using the primers listed in Supplementary Table S2 (Fig. 1A).

The authentication of HEK293T cells was verified by short tandem repeat analysis (Supplementary Table S3). The cells were transfected with 2.5 µg of the selected minigene plasmids using Lipofectamine 2000 DNA Transfection Reagent (Invitrogen, Carlsbad, CA, USA). After 48 hours, the total RNA was extracted using the RNAprep Pure Cell/Bacteria Kit (Tiangen Biotech, Beijing, China) and utilized for reverse transcription (RT)-PCR with primers in the exons V1 and V2 of pET01 (ETPR04 and ETPR05) and the FastKing One-Step RT-PCR Kit (Tiangen Biotech).[15] The products were separated by electrophoresis on 2% agarose gels, excised, and sequenced. Densitometric analysis of the gel electrophoresis images was performed using ImageJ software (National Institutes of Health, Bethesda, MD, USA) to assess the quantity of differently spliced products, which were the mean values of three independent repeated experiments.[16]

We also performed RT-PCR analysis from patient-derived peripheral blood mononuclear cells (PBMCs) from two patients (010408 carrying p.L40P/c.1101-491A>G and 010740 harboring p.R47L/c.867+97G>A) and one unrelated normal control (WT/WT) to validate the minigene assay results. Total RNA extraction and RT-PCR reactions were essentially as described for the minigene assay. The specific primer pairs for *BEST1* and *GAPDH* (internal control) to amplify the cDNA products are listed in Supplementary Table S2.

The DIVs c.867+97G>A/T in transcript NM_004183.4 are missense variants c.646G>A/T (p.V216I/F) and c.964G>A/T (p.V322I/F) in another two annotated transcripts, ENST00000526988.1 and ENST00000524926.5. We performed RT-PCRs using a pair of primers in normal human retina, induced pluripotent stem cell-derived (iPSC)-RPE cells, and PBMCs to amplify transcript products encompassing exon 3 to exon 9 (Supplementary Table S2). The postmortem adult human retina of a 45-year-old male donor who had died within 24 hours was obtained from the Eye Bank of Beijing Tongren Hospital. The generation of the iPSC line from a urine sample and differentiation into iPSC-RPE cells were performed as described elsewhere.[17,18] We collected mature iPSC-RPE cells on day 84 (see Supplementary Materials).

Haplotype Analysis

Eleven intragenic single nucleotide polymorphisms (SNPs) flanking c.867+97G>A were selected to analyze the haplotype in 17 unrelated patients harboring homozygous (n = 2) or heterozygous (n = 15) c.867+97G>A variants. The SNPs (rs972355, rs972354, rs972353, rs1800007, rs1801393, rs1109748, rs760306, rs195162, rs195161, rs1800009, and rs17156609) spanning a region of 14.64 kb were located upstream of exon 1, exon 2, exon 3, exon 5, and exon 10 and downstream of exon 11 in the *BEST1* gene. The SNPs were amplified by PCR and analyzed by Sanger sequencing using the primers shown in Supplementary Table S1.

We chose ethnically matched Chinese Han Beijing (CHB) and Chinese Han South (CHS) populations from the 1000 Genomes Project (https://www.internationalgenome.org/) as the normal controls. The haplotypes were constructed in patients and normal controls using the EM algorithm and the Haploview 4.2 program (https://www.broadinstitute.org/haploview/), which further calculated the frequencies of different haplotypes.

Statistical Analysis

Statistical analysis was performed using Prism 8.0.2 (GraphPad Software, San Diego, CA, USA). Either χ^2 or Fisher's exact test was applied to compare the categorical data of two independent samples. $P < 0.05$ was considered statistically significant.

Results

BEST1 Gene Variants

We identified 54 distinct *BEST1* pathogenic variants in 63 families, which included 62 pedigrees with biallelic variants and one family with only one variant detected (Supplementary Table S4). Sanger sequencing of *BEST1* initially detected 51 variants, whereas subsequent WGS revealed three missing variants in the introns. The 54 variants included 36 missense, four nonsense, three DIVs, three splicing, three small indel frameshifts, two in-frame deletions, two synonymous, and one regulatory region variant (Fig. 2A). These variants are broadly distributed in exons 2 to 9 and 11; however, almost 65% of the variants were clustered in exons 2, 5, 7, and 8 (Fig. 2B), which formed three hotspot regions (I, 12–52 aa; II, 184–205 aa; and III, 253–312 aa) (Fig. 2C). Over 75% of the missense variants were located in the three hot regions, and the truncated variants were mainly distributed in hot regions I and III, which corresponded to transmembrane domain 1 (TM1) and TM4 (Fig. 2C). Among the 54 putative causative variants, 11 were first identified in the current cohort. The novel variants either were absent in our in-house database or several public databases, such as the 1000 Genomes, GnomeAD, and ExAC databases, or were present at very low frequencies (Supplementary Table S5). The variants included 13 common variants (occurring three times or more), and the four most common variants were c.867+97G>A, p.R255W, p.Y44H, and p.A195V, with allele frequencies of 16% (20/125), 12.8% (16/125), 5.6% (7/125), and 5.6% (7/125), respectively (Table 2).

Investigative Ophthalmology & Visual Science

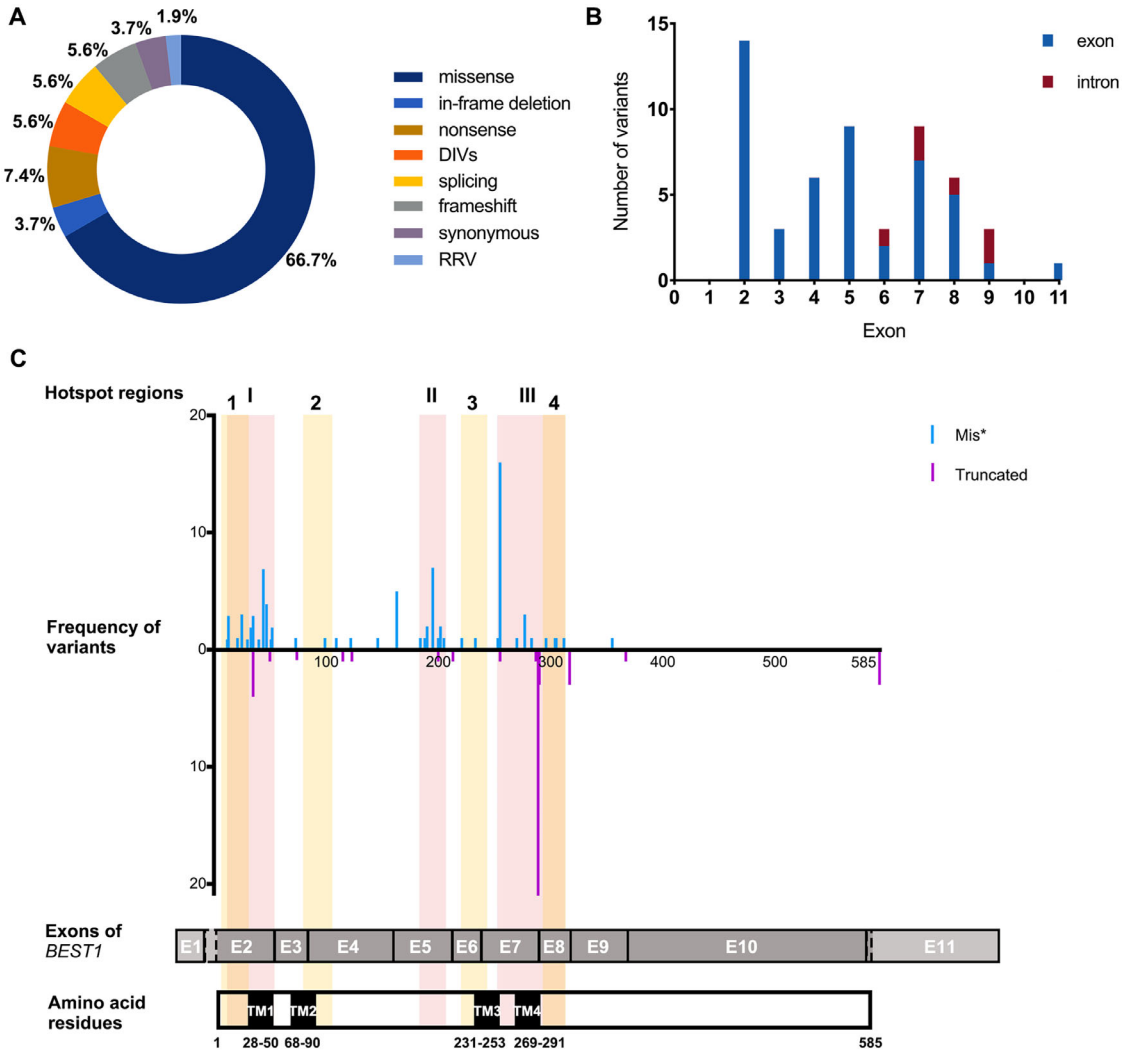

Figure 2. Summary of the variants identified in this study. (**A**) Proportion of different variant types. (**B**) The variant numbers identified for each of 11 exons. (**C**) The distribution of 54 distinct variants of *BEST1* in this study. The locations of hot regions I to III for ARB (*pink vertical bars*) and four well-known hot regions 1 to 4 for Best vitelliform macular dystrophy (BVMD) (*yellow vertical bars*) are shown relative to the exons of the *BEST1* gene and the protein sequence. The overlapped areas are indicated in *orange*. *Blue bars* (Mis*) indicate missense or in-frame deletion variants; *purple bars* indicate truncated variants (nonsense, deep intronic variants [DIVs], splicing, frameshift, synonymous, and regulatory region variants [RRVs]). For exons of *BEST1*, *dark gray* indicates an open reading frame and *light gray* represents an untranslated region.

Table 2. Common Variants Detected in This Cohort

Exon/Intron	Nucleotide Change	Protein Effect	Allele No. (%)
Intron 7	c.867+97G>A	p.[Ala291Glyfs*146,=]	20 (16)
Exon 7	c.763C>T	p.(Arg255Trp)	16 (12.8)
Exon 2	c.130T>C	p.(Tyr44His)	7 (5.6)
Exon 5	c.584C>T	p.(Ala195Val)	7 (5.6)
Exon 5	c.488T>G	p.(Met163Arg)	5 (4)
Exon 2	c.102C>T	p.[=, Glu35Trpfs*9]	4 (3.2)
Exon 2	c.38G>A	p.(Arg13His)	3 (2.4)
Exon 2	c.73C>T	p.(Arg25Trp)	3 (2.4)
Exon 2	c.103G>A	p.(Glu35Lys)	3 (2.4)
Exon 2	c.140G>T	p.(Arg47Leu)	3 (2.4)
Exon 7	c.830C>T	p.(Thr277Met)	3 (2.4)
Intron 7	c.868-2A>G	p.(=)	3 (2.4)
Exon 11	c.*24C>T	p.(=)	3 (2.4)

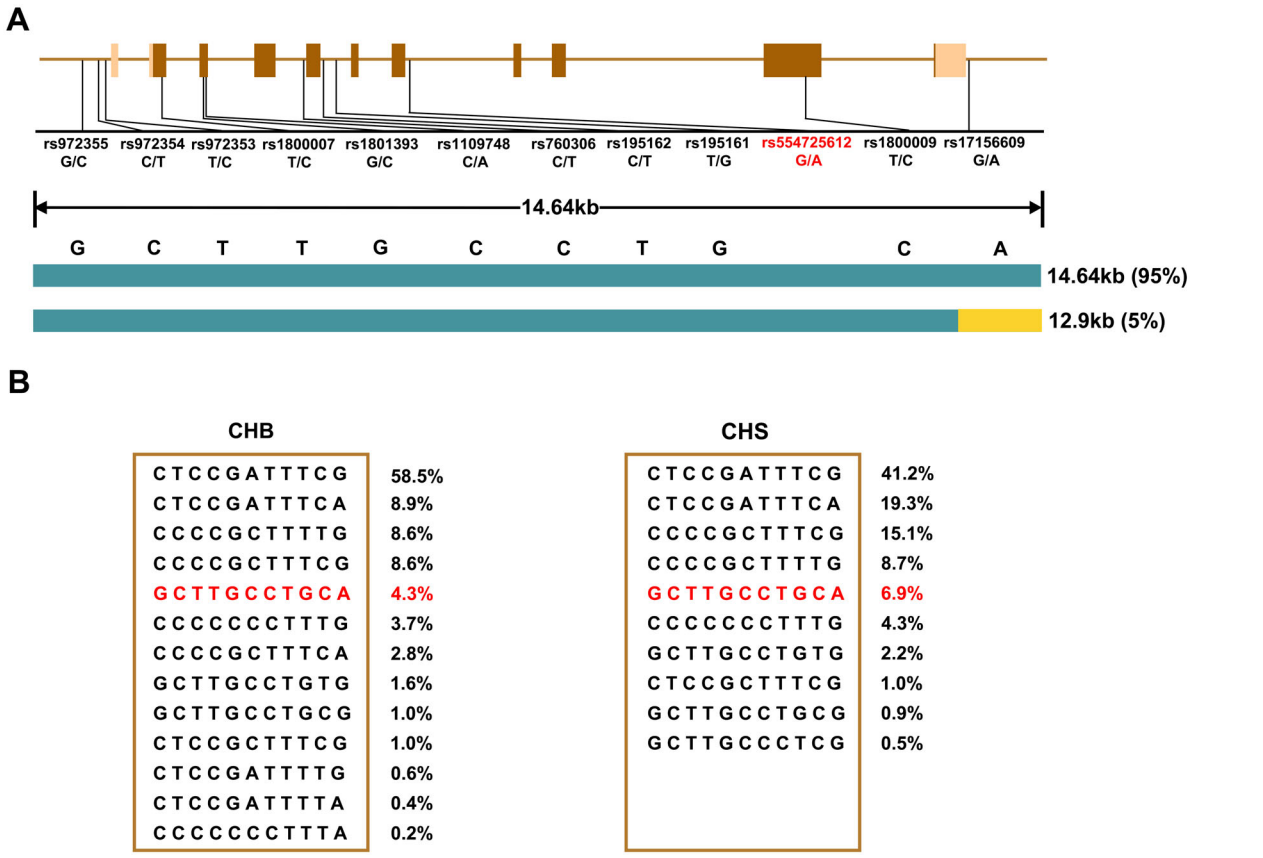

Figure 3. Haplotype analysis in 17 patients carrying the c.867+97G>A variant. (**A**) A schematic diagram showed 11 single nucleotide polymorphisms (SNPs) encompassing the *BEST1* gene and two haplotypes in mutant chromosomes with c.867+97G>A. The ancient haplotype (GCTTGCCTGCA) is colored *green* and accounted for 95% of the mutant chromosomes. Another haplotype (GCTTGCCTGCG) showing recombination (*yellow*) from the ancient haplotype accounted for 5%. (**B**) Haplotypes in healthy controls from the CHB and CHS populations. The GCTTGCCTGCA haplotype was detected at 4.3% and 6.9%, respectively.

Minigene Assay and RT-PCR Analysis

The RT-PCR analysis from both the minigene assay and patient-derived PBMCs indicated that DIV c.1101-491A>G generated abnormal splicing products (B1 and B6) (Figs. 1B, 1D). Consistent with the prediction by bioinformatic analyses, the aberrant products embraced an insertion of a 204-nt PE due to triggering a cryptic donor site. The aberrant transcript is assumed to create a premature termination codon (PTC), p. (Ser367Argfs*59), and might cause mRNA degradation by nonsense-mediated decay (NMD). The RT-PCR results from the minigene assay and PBMCs showed that DIV c.867+97G>A/T and WT both had two splicing or transcript products (Figs. 1C, 1E). The bands B5 and B9 corresponded to the normal splicing products, and the bands B4 and B8 contained a 203-nt IR, which is presumed to disrupt the reading frame and result in a PTC p. (Ala291Glyfs*146) or another *BEST1* transcript. Densitometric analysis of the minigene results (semiquantitative analysis) showed ratios of the abnormal transcript in total transcripts of 67.7%, 50.0%, and 37.5% for the DIV c.867+97G>A, c.867+97G>T, and WT constructs, respectively. These ratios were 44.4% and 28.6% based on the RT-PCR results from the PBMCs of the patient carrying heterozygous c.867+97G>A and the normal control, suggesting that c.867+97G>A/T strengthened the alternative donor site in intron 7 and produced more aberrant products (Figs. 1C, 1E). Moreover, our RT-PCR results from the human retina, iPSC-RPE, and PBMCs all displayed two transcript products. The subsequent sequencing revealed that the shorter band corresponded to the transcript isoform NM_004183.4, whereas the longer band was in line with transcript ENST00000524926.5 (Fig. 1F, Supplementary Fig. S2).

Haplotype Analysis

Intragenic SNP haplotype analysis revealed two different haplotypes, GCTTGCCTGCA (95%) and GCTTGCCTGCG (5%), in mutant chromosomes with c.867+97G>A, and 13 and 10 SNP haplotypes were found in CHB and CHS normal controls, respectively (Supplementary Table S6, Fig. 3). The GCTTGCCTGCA haplotype was predominant in the 17 patients but rare in the CHB and CHS populations, with frequencies of 4.3% and 6.9%, respectively. The haplotype difference between the patients harboring c.867+97G>A and the normal CHS and CHB population was assessed as statistically significant with Fisher's exact test ($P < 0.001$).

Clinical Findings

In this cohort, co-segregation analysis revealed that 62 probands (34 males and 28 females) carried biallelic variants of *BEST1*. Their mean age at last examination was 28.0 ± 13.8 years (range, 3.8–61.3). Almost all patients

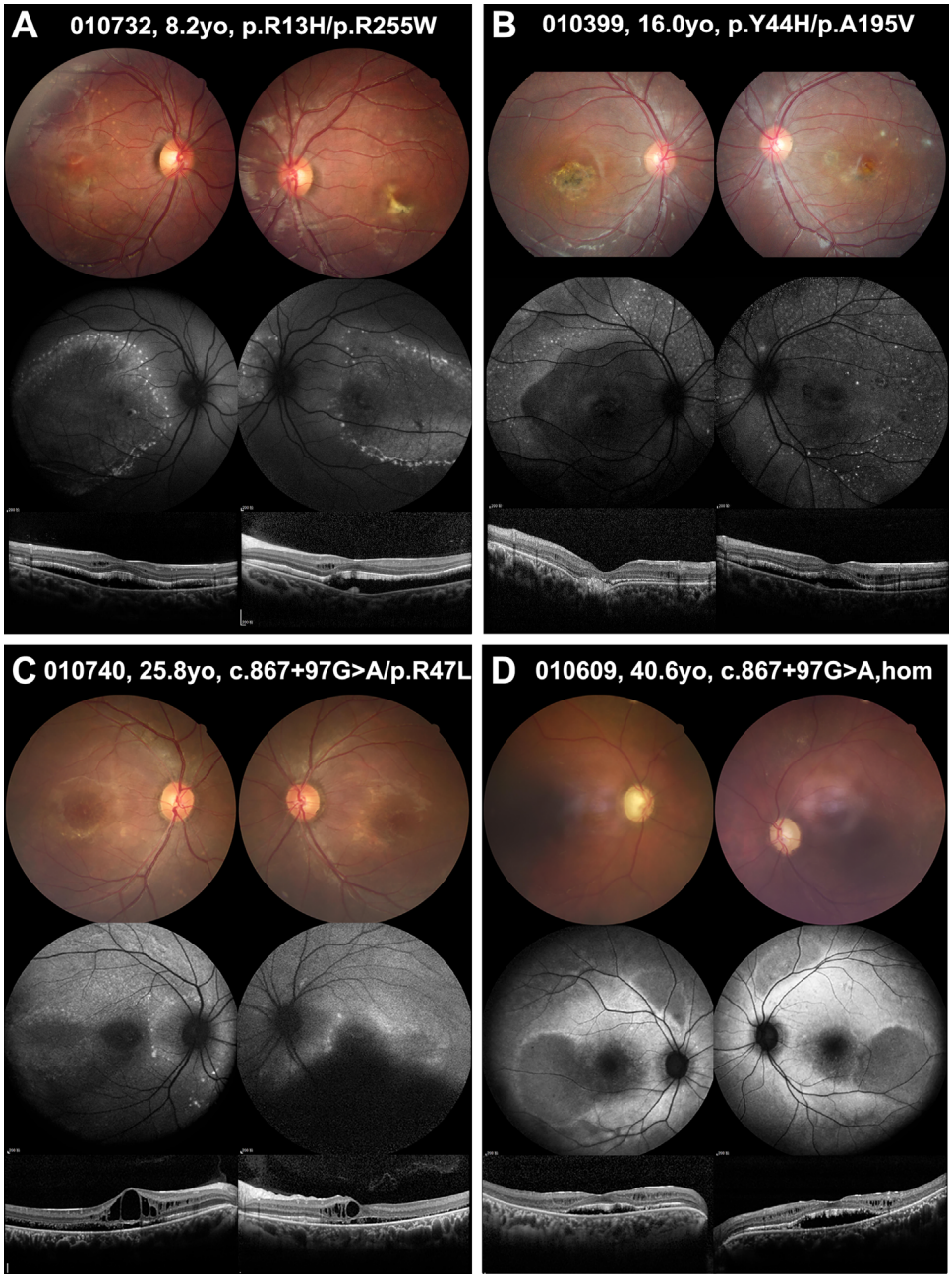

Figure 4. Colored fundus (CF) photographs, fundus autofluorescence (FAF), and spectral-domain optical coherence tomography (SD-OCT) images of patients with typical retinal features. (**A**, **B**) Patients 010732 and 010399 (younger than 20 years of age) showed subretinal yellowish flecks or dots in CF, corresponding to the hyper-autofluorescence encircling the vascular arcades on FAF. Retinal scars were obvious in the left eye of 010732 and the right eye of 010399. OCT exhibited elongated outer segments of the photoreceptors, cystoid macular edema, and subretinal fluid. The Bruch membrane in the right eye of 010399 was ruptured and contained a hyperreflective substance. (**C**, **D**) Patients 010740 and 010609 (older than 20 years) presented diffuse and punctate lesions in CF and extensive hyper-autofluorescence in the posterior pole of the retina, with finer hyper-autofluorescence around the arcades and disc on FAF. OCT scanning revealed obvious outer segment loss of the photoreceptors in the temporal retina and retinoschisis. Patient 010609 presented with an enlarged cup/disk ratio of 0.8 in the right eye. yo, years old.

experienced reduced vision. Some patients also had metamorphopsia, night blindness, and squint. Their clinical features are displayed in Supplementary Table S4. The patients younger than 20 years showed subretinal yellowish flecks or dots corresponding to the hyper-autofluorescence that encircled the vascular arcades on their FAF. The OCT examinations indicated elongated outer segments of the photoreceptors and the presence of cystoid macular edema (CME) and SRF (Figs. 4A, 4B). The patients older than 20 years of age presented more diffuse and punctate lesions and extensive hyper-autofluorescence in the posterior pole of the retina, with finer hyper-autofluorescence around the arcades and disc on their FAFs. OCT scans revealed a denser ellipsoid and interdigitation zones in the macular and nasal

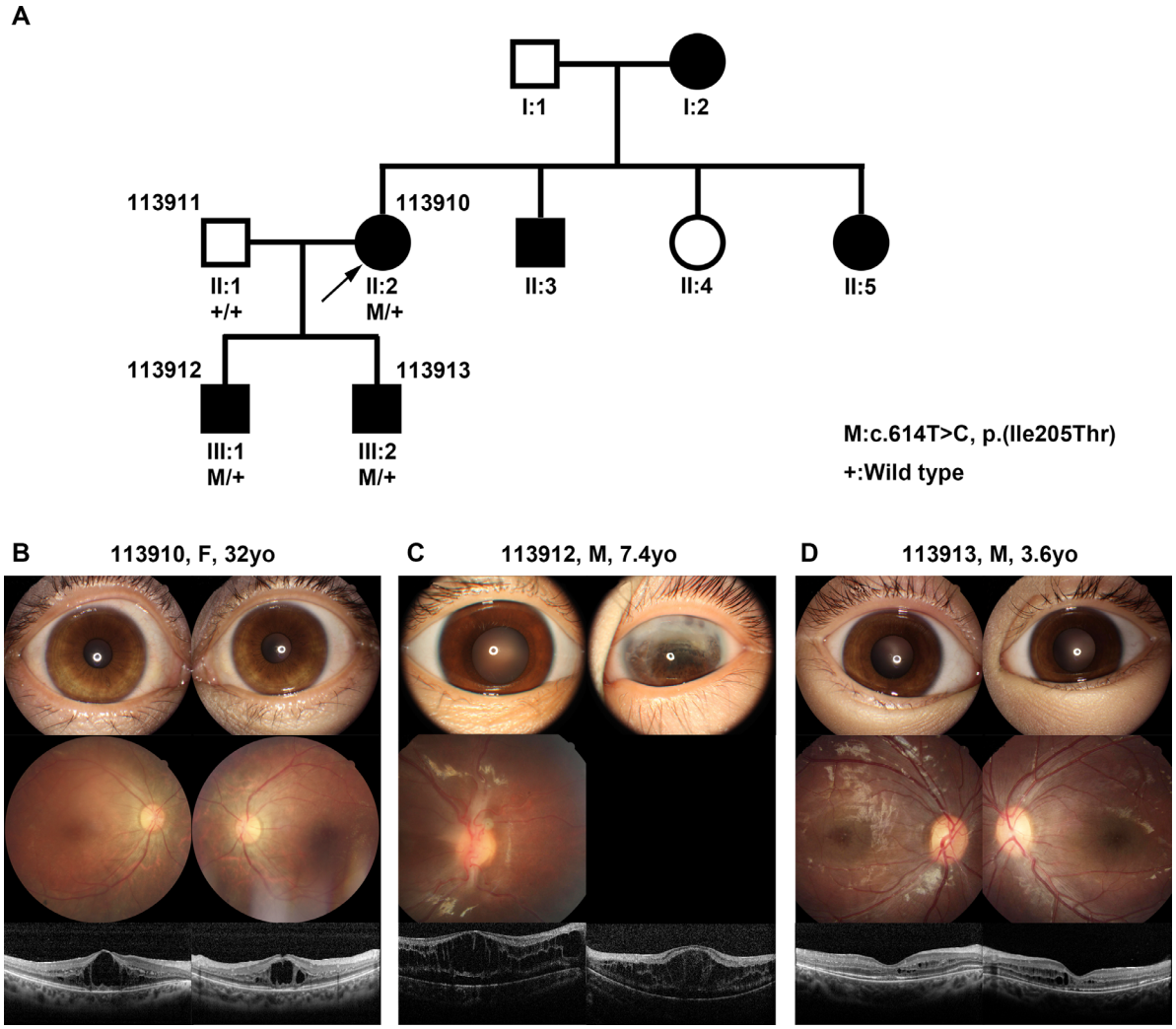

Figure 5. Genetic analysis and ophthalmic examinations of the autosomal dominant (AD) family. (**A**) Pedigree and co-segregation analysis. (**B**) Ophthalmic examinations of proband 113910. Anterior segment photographs showed mild atrophy of the iris stroma in both eyes. Fundus photographs showed attenuated retinal arteries, hypopigmented fovea, mild RPE atrophy, and scattered hyperpigmentation in the mid-peripheral retina. Optical coherence tomography (OCT) revealed cystoid macular edema and a mildly elongated photoreceptor outer segment. (**C**) Ophthalmic examinations of patient 113912. Anterior segment photographs showed leukoma in the left eye, but normal in the right eye. Fundus photographs of the right eye demonstrated a pale disk and mild pigment changes around the disk. OCT showed extensive retinoschisis and retinal detachment in both eyes. (**D**) Ophthalmic examinations of patient 113913. Anterior segment photographs showed mild atrophy of the iris stroma in both eyes. Fundus photographs revealed a wheel pattern in the macula in both eyes. OCT showed widespread intraretinal cystoid changes and an elongated photoreceptor outer segment. yo, years old.

retinal regions but a loss of the photoreceptors in the temporal retina (Figs. 4C, 4D). More than half of the patients showed excavated optic discs, enlarged cup-to-disk ratios, and/or retinal nerve fiber layer defects (Fig. 4D).

A Monoallelic Variant c.614T>C Identified in an AD Family

In the current cohort, three affected members from family (113910) had only one pathogenic variant detected. The Mongolian ethnicity family had six affected members, and three were clinically evaluated in our hospital (Fig. 5A). The proband (113910, a 32-year-old woman) and her younger son (113913, 3.6 years old) were diagnosed with ARB based on findings of CME and a mild elongated photoreceptor outer segment observed in OCT (Figs. 5B, 5D). Patient 113912 (7.4 years old), another son of the proband, was diagnosed with congenital glaucoma and bilateral retinal detachment (RD) at the age of 6 months. He showed leukoma in the left eye and extensive retinoschisis and RD in both eyes at his last examination at our hospital (Fig. 5C). WGS of the proband and her son did not identify any other pathogenic variant except a heterozygous variant, c.614T>C (p.I205T), initially detected in the Sanger sequencing of the *BEST1* gene.

Discussion

In this study, we conducted comprehensive genetic analyses and defined the variant landscape of *BEST1* in a large cohort with ARB. We observed that 33.3% of the pedigrees had one or no variant identified after Sanger sequencing of the *BEST1* gene; this rate was consistent with previous

Investigative Ophthalmology & Visual Science

observations (14%–59%) in several other studies.[10–12] The WGS analysis detected three DIVs in the *BEST1* gene and unraveled the missing heritability in 20 of the 21 families (95%) in the current cohort. Our results highlight the importance of screening the noncoding region when analyzing the variants of *BEST1*.

The 54 distinct variants identified in this study comprised all types of pathogenic *BEST1* variants, except for copy number variations, which were only reported in three patients.[12,19,20] Most variants (67%) were missense, in agreement with our previous observations and several other studies (58%–88%)[9,10,21–23]; however, this percentage of missense variants identified in patients with ARB was much lower than the percentage (94.7%–100%) detected in patients with BVMD.[9,10,23] The variants detected in our cohort were mainly clustered in three hotspot regions: codons 12 to 52, 184 to 205, and 253 to 312. These hotspots differed from the four well-known hot regions for BVMD described previously by Krämer et al.[24] In the current cohort, the most common variant was c.867+97G>A, with an allele frequency of 16%. This was a missing variant revealed by WGS and could explain the frequent occurrence of patients with only one or no variant in our previous study and in other studies that had included Chinese patients with ARB.[10–12]

The three DIVs described in the current study were the first DIVs identified in the *BEST1* gene. In line with our previous results for the *ABCA4* and *WFS1* genes,[15,25] the RT-PCR results for in vitro functional assays and for PBMCs from patients showed that the novel DIV c.1101-491A>G activated a cryptic splice donor site to generate aberrant splicing products that resulted in a PE insertion. The PE insertion changed the reading frame and caused a PTC. By contrast, the DIVs c.867+97G>A and c.867+97G>T caused a 203-nt IR by strengthening an alternative donor site in intron 7. The IR also altered the reading frame and generated a PTC, suggesting that all three DIVs caused ARB due to a haploinsufficiency mechanism. We observed that both the DIV c.867+97G>A/T and WT produced normal and abnormal products, but semiquantitative analysis revealed that the fractions of mutant transcripts were much higher in the DIVs than in the WT. The variant c.867+97G>A was previously detected in a heterozygous state in one Indian family and a homozygous state in a Chinese family with ARB, but it was defined as a missense variant, c.646G>A (p.V216I), in transcript ENST00000526988.[26,27] The so-called missense variant was predicted to be benign by two in silico tools.

To date, eight transcript isoforms were annotated in Ensembl (release 75). Our RT-PCR analysis in the normal human retina, iPSC-RPE, and PBMCs showed two transcript isoforms: The short isoform corresponded to NM_004183.4, and the long isoform corresponded to ENST00000524926.5 (but not ENST00000526988). The expression level was higher for transcript NM_004183.4 than for ENST00000524926.5. This, unsurprisingly, was more obvious in the iPSC-RPE, as *BEST1* is predominantly expressed in the RPE.[3] Furthermore, only the 585-aa bestrophin 1 encoded by the transcript NM_004183.4 has been described,[2,3] whereas the long isoform ENST00000524926.5 contained an extra 203-nt of intron7 that could lead to a PTC after 146 amino acids and finally trigger an NMD.

Our semiquantitative analysis indicated that DIV c.867+97G>A/T produced more abnormal splicing products than the WT, but the results did not fully reflect the real condition in the RPE. This difference in splicing outcomes between different cell types has been reported in previous studies involving the DIVs in *ABCA4* and *CEP290*.[28,29] Thus, patient-derived iPSC-RPE would be an appropriate cellular system for future analyses of splice defects of DIVs.

Haplotype analysis identified the common variant c.867+97G>A as a founder variant for Chinese patients with ARB; it was associated with two haplotypes: a 14.64 kb haplotype (GCTTGCCTGCA) covering the whole *BEST1* gene and a 12.9 kb haplotype encompassing region from upstream of exon1 to exon10 (rs1800009). Most of the mutant alleles (95%, 18/19) were associated with the 14.64 kb haplotype, and the significantly higher percentage than the rate (4.3 or 6.9%) in the normal Chinese controls suggested that the c.867+97G>A might have arisen from a single ancestor. Only one mutant allele was associated with the 12.9-kb haplotype, which might have been generated from the ancient founder haplotype by one or two recombination consequences.

In the current cohort, only one family (113910, containing three patients) was found to carry one missense variant p.I205T. The three patients presented fundus appearances that resembled ARB; a similar phenotype was described in three Italian patients of one four-generation family carrying the same variant and was defined as ARB-like.[30] Consistent with family 113910, the ARB-like phenotype in the Italian pedigree was transmitted in an autosomal-dominant mode.[30] In addition to the ARB-like phenotype, patient 113912 suffered a retinal detachment and congenital glaucoma, and the proband of the Italian pedigree presented severe atypical retinal phenotype, including obvious atrophy in the posterior pole, uneven hyperpigmentation in the peripheral retina, extensive epiretinal membrane, and vitreous condensations.[30] In another previous study, the variant p.I205T was also identified in a patient with a fundus appearance resembling that observed in patient 113912.[31] The high-resolution cryogenic electron microscopy (cryo-EM) structures of human bestrophin 1 resembled pentameric assembly and retained two landmark permeation constrictions: the neck and aperture, the later formed by residues I205/Q208/N212.[32] This latest study revealed that residue I205 was situated in the narrowest point of the aperture in the ion-conducting pathway.[32] One early in vitro study also found that variant p.I205T produced markedly decreased chloride currents in HEK293T cells even in the heterozygous state.[31] All of these findings suggest that variant p.I205T could cause a wide spectrum of ocular phenotypes ranging from ARB-like phenotype to early-onset vitreoretinal degeneration and anterior segment dysplasia in an AD pattern.

In conclusion, our results expand the pathogenic variant spectrum of *BEST1* and indicate that DIVs can explain almost all the missing heritability for Chinese patients with ARB. DIV c.867+97G>A contributed 16% of the heritability in this cohort and is a common founder variant for Chinese patients with ARB. Our findings may open up a new treatment strategy for patients carrying these DIVs.

Acknowledgments

Supported by the National Key R&D Program of China (2017YFA0104103 and 2016YFC0905200). The funding organization had no role in designing or conducting this research.

Disclosure: **J. Shi**, None; **L. Tian**, None; **T. Sun**, None; **X. Zhang**, None; **K. Xu**, None; **Y. Xie**, None; **X. Peng**, None; **X. Tang**, None; **Z.-B. Jin**, None; **Y. Li**, None

Investigative Ophthalmology & Visual Science

References

1. Burgess R, Millar ID, Leroy BP, et al. Biallelic mutation of *BEST1* causes a distinct retinopathy in humans. *Am J Hum Genet.* 2008;82:19–31.
2. Johnson A, Guziewicz K, Lee C, et al. Bestrophin 1 and retinal disease. *Prog Retin Eye Res.* 2017;58:45–69.
3. Marmorstein AD, Marmorstein LY, Rayborn M, Wang X, Hollyfield JG, Petrukhin K. Bestrophin, the product of the Best vitelliform macular dystrophy gene (VMD2), localizes to the basolateral plasma membrane of the retinal pigment epithelium. *Proc Natl Acad Sci USA.* 2000;97:12758–12763.
4. Marmorstein A, Kinnick T, Stanton J, Johnson A, Lynch R, Marmorstein L. Bestrophin-1 influences transepithelial electrical properties and Ca^{2+} signaling in human retinal pigment epithelium. *Mol Vis.* 2015;21:347–359.
5. Milenkovic A, Brandl C, Milenkovic V, et al. Bestrophin 1 is indispensable for volume regulation in human retinal pigment epithelium cells. *Proc Natl Acad Sci USA.* 2015;112:E2630–2639.
6. Marquardt A, Stöhr H, Passmore LA, Krämer F, Rivera A, Weber BH. Mutations in a novel gene, *VMD2*, encoding a protein of unknown properties cause juvenile-onset vitelliform macular dystrophy (Best's disease). *Hum Mol Genet.* 1998;7:1517–1525.
7. Allikmets R, Seddon JM, Bernstein PS, et al. Evaluation of the Best disease gene in patients with age-related macular degeneration and other maculopathies. *Hum Genet.* 1999;104:449–453.
8. Yardley J, Leroy B, Hart-Holden N, et al. Mutations of *VMD2* splicing regulators cause nanophthalmos and autosomal dominant vitreoretinochoroidopathy (ADVIRC). *Invest Ophthalmol Vis Sci.* 2004;45:3683–3689.
9. Wang Y, Jiang Y, Li X, et al. Genetic and clinical features of BEST1-associated retinopathy based on 59 Chinese families and database comparisons. *Exp Eye Res.* 2022;223:109217.
10. Tian L, Sun T, Xu K, Zhang X, Peng X, Li Y. Screening of *BEST1* gene in a Chinese cohort with Best vitelliform macular dystrophy or autosomal recessive bestrophinopathy. *Invest Ophthalmol Vis Sci.* 2017;58:3366–3375.
11. Xuan Y, Zhang Y, Zong Y, et al. The clinical features and genetic spectrum of a large cohort of Chinese patients with vitelliform macular dystrophies. *Am J Ophthalmol.* 2020;216:69–79.
12. Boon CJF, van den Born LI, Visser L, et al. Autosomal recessive bestrophinopathy: differential diagnosis and treatment options. *Ophthalmology.* 2013;120:809–820.
13. Liquori A, Vaché C, Baux D, et al. Whole *USH2A* gene sequencing identifies several new deep intronic mutations. *Hum Mutat.* 2016;37:184–193.
14. Bauwens M, Garanto A, Sangermano R, et al. *ABCA4*-associated disease as a model for missing heritability in autosomal recessive disorders: novel noncoding splice, *cis*-regulatory, structural, and recurrent hypomorphic variants. *Genet Med.* 2019;21:1761–1771.
15. Zhang X, Xie Y, Xu K, Chang H, Zhang X, Li Y. Comprehensive genetic analysis unraveled the missing heritability in a Chinese cohort with Wolfram syndrome 1: clinical and genetic findings. *Invest Ophthalmol Vis Sci.* 2022;63:9.
16. Schindelin J, Arganda-Carreras I, Frise E, et al. Fiji: an open-source platform for biological-image analysis. *Nat Methods.* 2012;9:676–682.
17. Zhang X, Zhang D, Thompson JA, et al. Gene correction of the *CLN3* c.175G>A variant in patient-derived induced pluripotent stem cells prevents pathological changes in retinal organoids. *Mol Genet Genomic Med.* 2021;9:e1601.
18. D'Antonio-Chronowska A, D'Antonio M, Frazer KA. In vitro differentiation of human iPSC-derived retinal pigment epithelium cells (iPSC-RPE). *Bio Protoc.* 2019;9:e3469.
19. Ellingford JM, Campbell C, Barton S, et al. Validation of copy number variation analysis for next-generation sequencing diagnostics. *Eur J Hum Genet.* 2017;25:719–724.
20. Dalvin L, Abou Chehade J, Chiang J, Fuchs J, Iezzi R, Marmorstein A. Retinitis pigmentosa associated with a mutation in *BEST1*. *Am J Ophthalmol Case Rep.* 2016;2:11–17.
21. Casalino G, Khan KN, Armengol M, et al. Autosomal recessive bestrophinopathy: clinical features, natural history, and genetic findings in preparation for clinical trials. *Ophthalmology.* 2021;128:706–718.
22. Luo J, Lin M, Guo X, et al. Novel *BEST1* mutations and special clinical characteristics of autosomal recessive bestrophinopathy in Chinese patients. *Acta Ophthalmol.* 2019;97:247–259.
23. Gao F-J, Qi Y-H, Hu F-Y, et al. Mutation spectrum of the bestrophin-1 gene in a large Chinese cohort with bestrophinopathy. *Br J Ophthalmol.* 2020;104:846–851.
24. Krämer F, Mohr N, Kellner U, Rudolph G, Weber BHF. Ten novel mutations in *VMD2* associated with Best macular dystrophy (BMD). *Hum Mutat.* 2003;22:418.
25. Tian L, Chen C, Song Y, et al. Phenotype-based genetic analysis reveals missing heritability of *ABCA4*-related retinopathy: deep intronic variants and copy number variations. *Invest Ophthalmol Vis Sci.* 2022;63:5.
26. Nguyen TT, Poornachandra B, Verma A, et al. Next generation sequencing identifies novel disease-associated *BEST1* mutations in bestrophinopathy patients. *Sci Rep.* 2018;8:10176.
27. Ye P, Xu J, Luo Y, Su Z, Yao K. Familial autosomal recessive bestrophinopathy: identification of a novel variant in *BEST1* gene and the specific metabolomic profile. *BMC Med Genet.* 2020;21:16.
28. Albert S, Garanto A, Sangermano R, et al. Identification and rescue of splice defects caused by two neighboring deep-intronic *ABCA4* mutations underlying Stargardt disease. *Am J Hum Genet.* 2018;102:517–527.
29. Parfitt D, Lane A, Ramsden C, et al. Identification and correction of mechanisms underlying inherited blindness in human iPSC-derived optic cups. *Cell Stem Cell.* 2016;18:769–781.
30. Toto L, Boon CJF, Di Antonio L, et al. Bestrophinopathy: a spectrum of ocular abnormalities caused by the c.614T>C mutation in the *BEST1* gene. *Retina.* 2016;36:1586–1595.
31. Davidson AE, Millar ID, Urquhart JE, et al. Missense mutations in a retinal pigment epithelium protein, bestrophin-1, cause retinitis pigmentosa. *Am J Hum Genet.* 2009;85:581–592.
32. Owji AP, Wang J, Kittredge A, et al. Structures and gating mechanisms of human bestrophin anion channels. *Nat Commun.* 2022;13:3836.

Investigative Ophthalmology & Visual Science